An Energy Recondensation Method Using the Discrete Generalized Multigroup Energy Expansion Theory

Lei Zhu and Benoit Forget
Massachusetts Institute of Technology
Department of Nuclear Science and Engineering
77 Massachusetts Avenue
Cambridge, MA

Abstract – In this paper, the discrete generalized multigroup (DGM) method was used to recondense the coarse group cross-sections using the core level solution, thus providing a correction for neighboring effect found at the core level. This approach was tested using a discrete ordinates implementation in both 1D and 2D. Results indicate that 2 or 3 iterations can substantially improve the flux and fission density errors associated with strong interfacial spectral changes as found in the presence of strong absorbers, reflector of mixed-oxide fuel. The methodology is also proven to be fully consistent with the multigroup methodology as long as a flat-flux approximation is used spatially.

I. Introduction

Deterministic neutron transport methods have relied quite heavily on the multigroup treatment of the energy variable. Continuous energy data is condensed in a more manageable multigroup format through multiple levels of approximation to eventually produce a corrected dataset (i.e. self-shielding) with which the core calculation can be performed efficiently. This multilevel approach generally assumes that strong spectral effects are local and can be approximated coarsely has the spatial size increases to reduce computational costs. As the level of heterogeneity increases in nuclear reactor core designs, this assumption is not always valid and requires some adjustments to the approach.

Recently, an iterative transport-diffusion methodology (IGDM) was developed by Roberts et *al* [1] for Light Water Reactor core analysis to improve the accuracy of the noted spectral effect They performed iterations between the lattice level and core level calculations to improve the condensation of the nuclear data by accounting for the effect of neighboring nodes. The method was tested on a set of two dimensional LWR mini-core benchmark problems and showed good improvement. Similarly, a combination of COMBINE unit cell calculations, one dimensional discrete ordinates transport calculations of SCAMP, and nodal diffusion calculations of PEBBED were implemented in the Idaho National Laboratory's deterministic code to account for the neighboring effects in core with long mean free paths [2]. COMBINE generates homogenized unit cell cross sections for each 1-D node which are used by SCAMP to solve for the flux distribution along the dimension. The obtained flux distribution is used to generate nodal diffusion parameters for core calculations.

In this paper, an alternate approach is proposed that can essentially eliminate the need for the lattice-to-core level iteration or even the need for lattice calculations altogether. This

new methodology builds on a previous study in which a Discrete Generalized Multigroup (DGM) energy expansion theory was developed [3][4]. The energy dependence of the angular flux was expanded into a set of flux moments using the discrete Legendre orthogonal polynomials (DLOP's) [5]. This approach provided an unfolded fine group flux for the cost of a coarse group calculation over whole core calculations. The purpose of this study is to develop a recondensation scheme to improve the nuclear data based on full core effects without the need to iterate with lattice level calculations. The unfolded fine flux of the DGM calculation is used to recondense the nuclear data and an iterative process can follow to further improve accuracy at the core level.

Unlike current approaches that iterate between transport at the lattice level and spatially homogenized diffusion at the core level, the methodology was tested using an S_N angular discretization without spatial homogenization at both the lattice and core level. This was done to facilitate the comparison between solutions and to eliminate the spatial complexities that would ensue from homogenization when removing the lattice calculations. This approach will thus facilitate coarse group core level transport calculations with accuracy comparable to fine group solutions, which can be seen as extending the lattice techniques to the whole core.

The paper is organized as follows. Section II reviews the DGM method and states the idea of the recondensation method. Section III provides computational results on both 1-D and 2-D light water reactor problems. Section IV discusses the dependence of the method on the spatial discretizations. Section V presents a conclusion and direction of future work.

II. Method Description

In this section, the DGM method is reviewed briefly for completeness, followed by the basic principles of the recondensation method, and a discussion of the multi-level approach.

II.1 Review of the DGM Method

The detailed derivation of the DGM can be found in [3]. The eigenvalue problem of the transport equation can be written as:

$$\vec{\Omega}\cdot\nabla\psi(\vec{r},\vec{\Omega},E)+\sigma_t(\vec{r},E)\psi(\vec{r},\vec{\Omega},E)=$$
$$\int_0^\infty dE'\int_{4\pi} d\vec{\Omega}'\sigma_s(\vec{r},\vec{\Omega}'\to\vec{\Omega},E'\to E)\psi(\vec{r},\vec{\Omega}',E')+\frac{\chi(\vec{r},E)}{4\pi k}\int_0^\infty dE'\int_{4\pi} d\vec{\Omega}'\nu\sigma_f(\vec{r},E')\psi(\vec{r},\vec{\Omega}',E'), \quad (1)$$

where the angular flux is represented by ψ with phase space variables: $\vec{r}$ for all three spatial components, $\vec{\Omega}$ for the solid and E for the energy. The total and fission macroscopic cross-sections, fission energy spectrum, and scattering kernel are represented respectively by σ_t, σ_f, χ and σ_s, respectively. In the DGM method, the

angular flux is expanded in energy using a discrete orthogonal basis set, namely the discrete Legendre orthogonal polynomials (DLOP's). After some algebra, the DGM equation of the transport equation is:

$$\vec{\Omega}\cdot\nabla\psi_{ig}(\vec{r},\vec{\Omega})+\sigma_{t,0g}(\vec{r})\psi_{ig}(\vec{r},\vec{\Omega})+\delta_{ig}(\vec{r},\vec{\Omega})\psi_{0g}(\vec{r},\vec{\Omega})=$$
$$\sum_{g'=1}^{G}\sum_{l=0}^{\infty}\sum_{m=-l}^{l}\frac{Y_{lm}^{*}(\vec{\Omega})}{4\pi}\sigma_{s,lm,i,g'\to g}(\vec{r})\phi_{lm,g'}(\vec{r})+\frac{\chi_{ig}(\vec{r})}{4\pi k}\sum_{g'=1}^{G}\nu\sigma_{f,g'}(\vec{r})\phi_{g'}(\vec{r}), \tag{2}$$

where ψ_{ig} is the i^{th} angular flux moment within coarse group g, and is defined as:

$$\psi_{ig}(\vec{r},\vec{\Omega})=\sum_{K_g=0}^{N_g-1}P_i(K_g,N_g-1)\psi(\vec{r},\vec{\Omega},K_g), \tag{3}$$

in which the angular flux is expanded using DLOP's within each coarse group g:

$$\psi(\vec{r},\vec{\Omega},K_g)=\sum_{i=0}^{N_g-1}a_iP_i(K_g,N_g-1)\psi_{ig}(\vec{r},\vec{\Omega}), \tag{4}$$

where $\Delta E_K\in\Delta E_g$, $K_g=0,...,N_g-1$ is the index of the fine energy group point within the coarse group g, N_g is the total number of fine group points within the coarse group g, $P_i(K_g,N_g-1)$ is the discrete Legendre polynomials and a_i is a normalization coefficient. The cross section moments in (2) are defined as:

$$\nu\sigma_{f,g'}(\vec{r})=\frac{\sum_{L_{g'}=0}^{M_{g'}-1}\nu\sigma_f(\vec{r},L_{g'})\phi(\vec{r},L_{g'})}{\sum_{L_{g'}=0}^{M_{g'}-1}\phi(\vec{r},L_{g'})}, \tag{5}$$

$$\sigma_{s,lm,i,g'\to g}(\vec{r})=\frac{\sum_{L_{g'}=0}^{M_{g'}-1}\phi_{lm}(\vec{r},L_{g'})\sum_{K_g=0}^{N_g-1}P_i(K_g,N_g-1)\sigma_{sl}(\vec{r},L_{g'}\to K_g)}{\sum_{L_{g'}=0}^{M_{g'}-1}\phi_{lm}(\vec{r},L_{g'})}, \tag{6}$$

$$\chi_{ig}(\vec{r})=\sum_{K_g=0}^{N_g-1}P_i(K_g,N_g-1)\chi(\vec{r},K_g), \tag{7}$$

$$\sigma_{t,0g}(\vec{r}) = \frac{\sum_{K_g=0}^{N_g-1} \sigma_t(\vec{r}, K_g)\phi(\vec{r}, K_g)}{\sum_{K_g=0}^{N_g-1} \phi(\vec{r}, K_g)}, \tag{8}$$

$$\delta_{ig}(\vec{r}, \vec{\Omega}) = \frac{\sum_{K_g=0}^{N_g-1} P_i(K_g, N_g - 1)\delta_g(\vec{r}, K_g)\psi(\vec{r}, \vec{\Omega}, K_g)}{\sum_{K_g=0}^{N_g-1} P_0(K_g, N_g - 1)\psi(\vec{r}, \vec{\Omega}, K_g)}, \tag{9}$$

where the perturbation of the collision term is defined from:

$$\sigma_t(\vec{r}, K_g) = \sigma_{t,0g}(\vec{r}) + \delta_g(\vec{r}, K_g). \tag{10}$$

The total cross-section perturbation term is introduced to provide numerical stability to the higher order equations.

In the above coefficients, $L_{g'} = 0, ..., M_{g'} - 1$ is the index of the fine energy group point within the coarse group *g'*, $M_{g'}$ is the total number of fine group points within the coarse group *g'*. The coarse group fluxes are defined as:

$$\phi_{g'}(\vec{r}) = \sum_{L_{g'}=0}^{M_{g'}-1} \phi(\vec{r}, L_{g'}), \tag{11}$$

$$\phi_{lm,g'}(\vec{r}) = \sum_{L_{g'}=0}^{M_{g'}-1} \phi_{lm}(\vec{r}, L_{g'}). \tag{12}$$

In Eq. (2), the leading order equation is decoupled from the higher order equations due to the properties of DLOP's, and thus is equivalent to the standard coarse group solution which is piecewise constant within each coarse energy group. Higher order equations are decoupled from each other and coupled only to the leading order solution. These fixed source equations can be solved with a much less computational effort compared to the leading order calculation.

II.2 Energy Recondensation

While the DGM method greatly improves the energy resolution and at the same time keeps a computational efficiency comparable to the coarse group calculation, the flux spectrum needed to generate cross section moments defined by Eqs. (5)-(10) is not known *a priori.* This flux can be approximated from lattice level calculations, which is

equivalent to the traditional multilevel approach. This inaccurate flux spectrum used to generate cross section moments is the main source of error in the DGM calculation.

Despite these inaccuracies, the unfolded flux spectrum provided by the DGM calculation was shown to be a very accurate estimate of the reference fine group solution. This indicates that the DGM solution can be used as a weighing function to regenerate improved cross-section moments. This process can be repeated iteratively at the core level with each iteration taking essentially the computational time of a coarse group calculation.

II.3 Initial spectrum guess

In the traditional approach of full core calculation, the fine group flux spectrum needed to generate coarse group cross sections is provided from a separate lattice calculation. The DGM method in [3] (without recondensation) adopted a similar approach. The disadvantage of this approach is that extra lattice calculations need be performed even thought the fine group lattice solution may not be an accurate estimate of the whole core flux spectrum.

The recondensation procedure provides a way to eliminate the assembly calculation. Instead of using the flux from assembly calculation as weighting function, we can simply use an appropriate initial guess to generate cross section moments. For example, the initial guess can be a combination of a Maxwellian spectrum in the thermal range, *1/E* in the resonance range and the fission spectrum in the fast range. Alternatively even a flat flux estimate would still converge, but the more accurate the initial guess of the flux, the less iteration will be required to get a suitable result.

The flow chart of Fig.1 clearly presents the new approach, while Fig. 2 illustrates the traditional approach. The starting point, just with like any other calculation, is with a fine group cross-section set with appropriate self-shielding. The initial flux guess can be estimated by any means and will be used to generate the coarse group moments. A DGM calculation thus ensues for both the 0^{th} order and higher order equations. The unfolded flux is then used to recondense the cross-sections to initiate the iterative process. The recondensation procedure stops when a convergence criterion is met, which was set as the root mean square (*rms*) error of the scalar flux from two consecutive iterations.

III. Computational Results

Section III.1 and III.2 presents 1-D and 2-D results for a S_N implementation. It should however be noted that the methodology is general and thus not limited to the presented solution scheme.

III.1 One-dimensional BWR core tests

A detailed description of the set of 1-D BWR cores can be found in [3], and an illustration of the cores and assemblies is plotted in Fig. 3. For the results presented here,

the first iteration (DGM method) parameters are computed from assembly calculations with reflective boundary conditions. The goal of the recondensation calculations is to reduce the errors associated with the coarse group representation with minimal iterations, thus improving the coarse group solution considerably. If one desires the fidelity of the fine group solution, solving the usual multigroup equations would be more efficient. A comparison is made between 47 group reference solutions for the three 1-D cores with a 2 group DGM calculation with a thermal cutoff at 0.625 eV and respective expansion orders of 34 and 11 in each group, thus preserving exactly the 47 group dataset. A S_{16} angular approximation is applied and the step difference (SD) method is used for the spatial sweep. In the power iterations and fixed source iterations, the flux is converged to within 10^{-5}. The eigenvalue is converged to within 10^{-6}. Vacuum boundary conditions are set on both sides of the core.

The recondensation calculations for all three cores with different number of iterations are performed. The root-mean-squared (*rms*) relative error and mean relative (*mre*) error of the scalar flux are defined as:

$$rms = \sqrt{\frac{\sum_{i=1}^{I}\sum_{h=1}^{H} RE(i,h)^2}{I \times H}}, \tag{13}$$

$$mre = \frac{1}{I \times H}\sum_{i=1}^{I}\sum_{h=1}^{H}\left[RE(i,h) \times \frac{\phi_2(i,h)}{\phi_{2,avg}} \right]. \tag{14}$$

The pointwise relative error and the average flux in the core are defined as:

$$RE(i,h) = \left| \frac{\phi_1(i,h) - \phi_2(i,h)}{\phi_2(i,h)} \right|, \tag{15}$$

$$\phi_{avg} = \frac{1}{I \times H}\sum_{i=1}^{I}\sum_{h=1}^{H}\phi(i,h), \tag{16}$$

where $\phi_1(i,h)$ and $\phi_2(i,h)$ are scalar fluxes compared with spatial index *i* and fine energy group index *h*. Similarly for the eigenvalue, we define the relative error between two calculations as:

$$RE_k = \left| \frac{k_1 - k_2}{k_2} \right|. \tag{17}$$

Computational results are given in Tables 1-4 for cores 1 and 3, respectively, for the first three iterations. The computational time of the fine group reference calculations is roughly 10 seconds for each core while it takes approximately 0.4 seconds for each DGM iteration on a Intel 2.4Ghz PC with no acceleration. Tables 1 and 2 clearly indicate the

benefit of doing a few iterations when performing coarse group calculations. Within a few iterations both the eigenvalue error and scalar flux error improve considerably. , i.e., the scalar flux *rms* error in core 1 is reduced from 3.2% to 0.54% and in core 3 from 15% to 2.6% by performing 3 iterations.

Full convergence of the recondensation process was also studied by stopping the iterations when the *rms* relative error of scalar flux between two consecutive iterations reached 10^{-5}, as shown in the flow chart in Fig. 1. It takes 26 iterations for core 1 to satisfy this criterion while it takes 87 iterations for core 3. Converging fully using the recondensation process is equivalent to solving the fine group calculation, but less efficiently. This study was performed to show the consistency of the discretization in reproducing the fine group results. The recondensation procedure is envisioned as a way to improve coarse group results with minimal cost, not as a way to fully converge the fine group solution.

Scalar flux *rms* relative errors and eigenvalue relative errors are plotted in Figs. 4-7 for cores 1 and 3. It can be observed that the *rms* errors of scalar flux show a smoother convergence trend than the relative errors of the eigenvalue, which is the reason the *rms* error of scalar flux was selected as the convergence criteria of the recondensation. The oscillation of the eigenvalue at the beginning is caused by an inaccurate weighting spectrum for the cross sections in the first few iterations. After a certain number of iterations when the flux spectrum becomes more accurate, the oscillation of the eigenvalue diminishes considerably.

It can also be observed that after many iterations, errors between two consecutive iterations decrease which indicates convergence of the algorithm itself, while errors between the DGM solution and the reference solution eventually plateaus to a level within the accuracy of the convergence criteria. In the power iteration of both the reference calculation and the 0^{th} order DGM calculation, as well as the fixed source iteration in the higher order calculations, the flux is converged to within 10^{-5}. The final converged recondensation flux has an *rms* error on the order of 10^{-4} which is around one order larger than 10^{-5} due to round-off errors in cross section moments generation where fluxes (with an error on the order of 10^{-5}) appear in both the numerator and denominator.

Figs. 6 and 7 indicate that for core 3, after about 40 iterations, errors between the DGM solution and the reference solution stops decreasing, which means that more DGM iterations will not improve the overall accuracy even though the *rms** error of the DGM has yet to converge to the prescribed criterion. An alternative would be to use the *mre** as a stopping criterion, which converges to 10^{-5} after 54 iterations. Core 3 is heavily loaded with Gadolinium thus presenting near zero flux regions which are very difficult to capture accurately with a coarse group expansion methodology.

Figs. 8-10 show the scalar flux in core 3 as a function of energy groups for a representative water region, fuel region, and fuel with Gd region, respectively. It can be observed from the first three iterations that the fluxes converge to the reference spectrum with an increasing number of iterations.

The flux update procedure proposed in [3] is performed in each iteration in order to eliminate all possible negative values in the unfolded fluxes, which is very important when regenerating cross section moments for the next iteration. Eigenvalue updates were not performed in the iteration process to simplify the algorithm.

III.2 Two-dimensional PWR core tests

For a better assessment of the performance of this algorithm, a more realistic 2D PWR problem was used. The geometry and boundary conditions are similar to the C5G7 benchmark problem [6], and the core layout is plotted in Fig. 11. The circle fuel pin geometry is approximated in Cartesian geometry as indicated by the ORNL and GRS participants in [6], and is plotted in Fig. 12. Instead of the provided 7 group cross-section database, a 33 group self-shielded library was generated for both UO_2 and MOX fuels using DRAGON [7]. A comparison is made between 33 group reference solutions for the 2-D cores with a 2 group (with thermal cutoff of 4eV) DGM calculation with respective expansion orders of 28 and 3. A S_4 angular approximation is applied and the step difference method is again used for the spatial sweep. Both the reference and DGM calculations are performed using the same spatial mesh. Flux is converged to within 10^{-5}, and the eigenvalue is converged to within 10^{-6} in the power iterations. The initial flux spectrum guess is obtained from infinite assembly fine group calculations. Flux updates are performed at each iteration to eliminate all possible negative values in the unfolded fluxes, as was done in the 1-D tests.

In the 2-D problem, errors are defined as was done previously. Results are provided in Tables 5-7. Table 5 lists the *rms* and *mre* errors of the flux compared to the fine group solution, and the *rms** error between two consecutive DGM iterations which is used as the convergence criteria of the recondensation procedure. The recondensation process converges after 20 iterations when *rms** between two consecutive iterations is smaller than 10^{-5} (10^{-3}%). It can be observed that *rms* and *mre* errors decrease from 47% and 7.6% to 14% and 0.63%, respectively, after 3 iterations. *mre* errors are typically smaller than *rms* error which indicates that larger errors mainly exist in areas with near zero fluxes.

Table 6 lists the root-mean-square error (*rms*), mean relative error (*mre*), and maximum relative error (err_{max}) of the pin fission densities compared to the fine group solution, where the pin fission densities are defined as:

$$P = \sum_{j=1}^{J_{pin}} \sum_{i=1}^{I_{pin}} \sum_{h=1}^{H} \phi(i, j, h)\sigma_f(i, j, h), \tag{18}$$

where I_{pin}, J_{pin} and H are number of spatial meshes in x and y directions in a pin, and number of fine groups. The definition of the *rms* error, *mre* error and relative error are the same as for the flux errors except that the spatial mesh index is replaced by the fuel pin index. The err_{max} is the maximum of the relative error in absolute value of all the pins.

Errors of *rms*, *mre* and err_{max} in the first iteration solution are 7.3%, 6.0% and 24.1%, respectively, while they decrease to 0.72%, 0.3% and 3.8% after 3 iterations. Once again, the *mre* error is smaller than *rms* error in each iteration, indicating that larger errors are located in pins with low fission densities.

Table 7 lists the computational time and eigenvalues errors where RE_k* is the relative error between two consecutive DGM iterations and RE_k is the relative error between DGM and fine group solutions. The computational time of the fine group reference calculation is about 100 minutes, while each DGM iteration takes about 5 minutes. Comparing to the reference solution, relative error of eigenvalue is 1.3% after the 1st iteration and it decreases to 0.028% after 3 iterations.

Figs. 13-14 plot the errors on flux and eigenvalue as a function of the number of iterations. Once again, both the flux and eigenvalue converge to the fine group solution after 20 iterations. The *rms* errors of scalar flux show a smoother convergence trend than the relative errors of the eigenvalue.

Figs. 15-17 plots the relative error of pin power compared with the reference solution, for the 1st, 2nd and 20th iterations of the DGM calculations, respectively. Fig. 15 shows that large errors of pin power exist near the interface of fuel assemblies and moderator regions, as well as near the interface of UO_2 and MOX assemblies. This is due to the fact that the cross section moments are generated using infinite assembly fine group solutions as the weighting flux, thus neglecting the neighboring effect between different assemblies and near the reflector. Since the flux used to generate cross section moments for the 2nd iteration comes from the first iteration solution which is a core level solution, errors near assembly interfaces are reduced substantially, which is shown in Fig. 16. After 20 iterations, the errors become quite small throughout the core as is shown in Fig. 17.

IV. Limitations from the spatial discretization methods

All the previous calculations are based on the step difference spatial discretization which assumes a piecewise constant flux over each spatial cell. These results show that the flux can converge to the fine group solution after a certain number of iterations, but unfortunately this is not the case for all spatial discretization. This section analyzes the spatial consistency of the DGM method and discusses some of its limitations.

IV.1 Spatial dependence of the DGM method

The cross sections and moments used in the $(k+1)^{th}$ recondensation iteration calculation are generated using fluxes from the k^{th} iteration. For a fully consistent derivation, the reaction rates from the fine group calculation and the 0th order coarse group solution should be equivalent after the recondensation calculation converges. In [3], the DGM method is derived without dependence of a particular spatial discretization. The purpose of the following analysis is to study the effect of spatial discretization on the consistency of the DGM model. An analysis of the fission term is given as follows and similar

conclusion can be derived for other terms in the transport equation. The coarse group fission cross section given in Eq. (5) can be written as:

$$\nu\sigma_{f,g'}^{k+1}(x) = \frac{\sum_{L_{g'}=0}^{M_{g'}-1} \nu\sigma_f(x, L_{g'})\phi^k(x, L_{g'})}{\sum_{L_{g'}=0}^{M_{g'}-1} \phi^k(x, L_{g'})}, \tag{19}$$

which is the fission cross section energy condensation weighted by the scalar flux. Without loss of generality, spatial dependence is represented in a 1-D Cartesian formalism.

The continuous energy transport equation in Eq. (1) is separated into equations within each coarse energy groups. Within a coarse energy group *g'*, if a fine group calculation is performed, the fission rate can be expressed as:

$$R_{f,g'}(x) = \sum_{L_{g'}=0}^{M_{g'}-1} \nu\sigma_f(x, L_{g'})\phi(x, L_{g'}) \tag{20}$$

If a coarse group (or 0th order of DGM) calculation is performed, the fission rate expressed in the coarse group equation is:

$$R_{f,g'}^{k+1}(x) = \nu\sigma_{f,g'}^{k}(x)\phi_{g'}^{k+1}(x) \tag{21}$$

where $\phi_{g'}^{k+1}(x)$ is the unknown to be solved in the *(k+1)th* iteration in the coarse group (0th order) equation. The key point is to verify that the reaction rates in Eqs. (20) and (21) are equivalent after convergence of the recondensation process, which can be expressed by:

$$\phi^k(x, L_{g'}) = \phi^{k+1}(x, L_{g'}), \tag{22}$$

where $\phi^k(x, L_{g'})$ is the unfolded scalar flux from the *k*th iteration of the DGM calculation.

a) Flat-flux approximation

If the spatial dependence is expressed explicitly, it can be observed that the equivalence exists only when the SD spatial discretization is used. In general, cross sections and moments are collapsed using the cell-averaged flux, e.g., Eq. (19) can be written as:

$$\nu\sigma_{f,I,g'}^{k+1} = \frac{\sum_{L_{g'}=0}^{M_{g'}-1} \nu\sigma_{f,I}(L_{g'})\phi_I^k(L_{g'})}{\sum_{L_{g'}=0}^{M_{g'}-1} \phi_I^k(L_{g'})}, \tag{23}$$

where I is the spatial cell index, and ϕ_I is the cell-averaged flux. In the SD method, fluxes are piecewise constant within each spatial cell, e.g., $\phi(x, L_{g'}) = \phi_I(L_{g'})$ in cell I. Thus, Eq. (20) can be written as:

$$R_{f,g'} = \sum_{L_{g'}=0}^{M_{g'}-1} \nu\sigma_{f,I}(L_{g'})\phi_I(L_{g'}). \tag{24}$$

Eq. (21) can be written as:

$$R_{f,g'}^{k+1} = \frac{\sum_{L_{g'}=0}^{M_{g'}-1} \nu\sigma_{f,I}(L_{g'})\phi_I^k(L_{g'})}{\sum_{L_{g'}=0}^{M_{g'}-1} \phi_I^k(L_{g'})} \phi_{g',I}^{k+1}. \tag{25}$$

where the coarse group flux can be expressed using fine group fluxes as:

$$\phi_{g',I}^{k+1} = \sum_{L_{g'}=0}^{M_{g'}-1} \phi_I^{k+1}(L_{g'}). \tag{26}$$

Eqs. (24) and (25) should be equivalent which indicates that the reaction rate is conserved, if Eq. (22) is satisfied, i.e.,

$$\phi_I^k(L_{g'}) = \phi_I^{k+1}(L_{g'}). \tag{27}$$

b) Linear-flux approximation

For higher order spatial discretization schemes, e.g., the first order method, we can write the spatial dependence of Eq. (20) within a spatial mesh as:

$$R_{f,g'}(x) = \sum_{L_{g'}=0}^{M_{g'}-1} \nu\sigma_{f,I}(L_{g'})\phi(x, L_{g'}), \tag{28}$$

while the spatial dependence of Eq. (21) within a spatial mesh is:

$$R_{f,g'}^{k+1}(x)=\frac{\sum_{L_{g'}=0}^{M_{g'}-1}\nu\sigma_{f,I}(L_{g'})\phi_I^k(L_{g'})}{\sum_{L_{g'}=0}^{M_{g'}-1}\phi_I^k(L_{g'})}\phi_{g'}^{k+1}(x), \tag{29}$$

where the cross section is generated using cell average flux. In this case, the coarse group flux with spatial details within a spatial mesh $\phi_{g'}(x)$ cannot be expressed using fine group fluxes within that coarse group, i.e., an equivalent form of Eq. (26) does not exist. By comparing Eqs. (28) and (29), it can be observed that they will have a different form no matter whether an equivalence of Eq. (26) is satisfied, which means that the reaction rate will converge to a different value.

With spatial details within a spatial mesh, other terms have similar inconsistency and thus the recondensation model will generate a solution with a systematic error compared to the fine group solution.

IV.2 Collision term

The collision term is treated differently due to the fact that a perturbation technique is applied in the derivation of the DGM method to increase stability, which is similar to the treatment of angular dependence of the collision term in the discrete ordinates equations proposed in [8]. The purpose of this section is to study the consistency of this approximation with the recondensation procedure. Continuous spatial dependence is used in the derivation in this section, but as stated in section IV.1, consistency is only obtained when using a flat-flux approximation. If the continuous energy transport equation is separated into coarse energy group equations, the Legendre moments of collision term within a coarse group *g* is:

$$R_{t,ig}(\vec{r},\vec{\Omega})=\sum_{K_g=0}^{N_g-1}P_i(K_g,N_g-1)\sigma_t(\vec{r},K_g)\psi(\vec{r},\vec{\Omega},K_g) \tag{30}$$

This term can be condensed as:

$$R_{t,ig}^{k+1}(\vec{r},\vec{\Omega})=\sigma_{t,ig}^{k}(\vec{r},\vec{\Omega})\psi_{ig}^{k+1}(\vec{r},\vec{\Omega}) \tag{31}$$

Where the angular flux moment is defined in Eq. (3) and the total cross section moment is defined as:

$$\sigma_{t,ig}^{k}(\vec{r},\vec{\Omega})=\frac{\sum_{K_g=0}^{N_g-1}P_i(K_g,N_g-1)\sigma_t(\vec{r},K_g)\psi^k(\vec{r},\vec{\Omega},K_g)}{\sum_{K_g=0}^{N_g-1}P_i(K_g,N_g-1)\psi^k(\vec{r},\vec{\Omega},K_g)} \tag{32}$$

With *i=0*, Eq. (31) is the total reaction rate condensed from fine group to coarse group using angular flux as the weighting function. However, a disadvantage of Eq. (31) is that the DLOP's appears in the denominator of the definition, which may lead to large round-off error and instability when generating $\sigma^k_{t,ig}(\vec{r},\vec{\Omega})$ moments. One way proposed in [9] and [3] is to use an averaged collision term together with a perturbation term such that:

$$\begin{aligned} R^{k+1}_{t,ig}(\vec{r},\vec{\Omega}) &= \sigma^k_{t,0g}(\vec{r})\psi^{k+1}_{ig}(\vec{r},\vec{\Omega}) + \delta^k_{ig}(\vec{r},\vec{\Omega})\psi^{k+1}_{0g}(\vec{r},\vec{\Omega}) \\ &= \sigma^k_{t,0g}(\vec{r})\sum_{K_g=0}^{N_g-1} P_i(K_g, N_g-1)\psi^{k+1}(\vec{r},\vec{\Omega},K_g) \\ &+ \frac{\sum_{K_g=0}^{N_g-1} P_i(K_g, N_g-1)\delta^k_g(\vec{r},K_g)\psi^k(\vec{r},\vec{\Omega},K_g)}{\sum_{K_g=0}^{N_g-1}\psi^k(\vec{r},\vec{\Omega},K_g)} \sum_{K_g=0}^{N_g-1}\psi^{k+1}(\vec{r},\vec{\Omega},K_g) \end{aligned} \tag{33}$$

If after many recondensation iterations, we obtain convergence such that:

$$\psi^k(\vec{r},\vec{\Omega},K_g) = \psi^{k+1}(\vec{r},\vec{\Omega},K_g), \tag{34}$$

It can be observed that Eq. (33) can be simplified to Eq. (30), which shows consistency of the derivation. If written explicitly the spatial dependence within a spatial mesh is satisfied only when a flat flux approximation is used. Thus, the perturbation term approximation of the collision term does not induce any extra error in the recondensation iterations for 0^{th} order spatial schemes. One major disadvantage that can be seen in Eq.(33) is the angular dependence of the collision rate which requires storing the angular flux. One way to solve this problem is to expand the angular dependence of angular flux in the perturbation term using Legendre polynomials, as indicated in [8].

V. Conclusions and Future Work

In this study, an energy recondensation methodology is developed based on the DGM energy expansion theory previously developed. Cross sections and moments are regenerated using the obtained DGM flux spectrum as weighting function at the beginning of each iteration. Computational tests are performed on one dimensional BWR cores with and without Gadolinium, and two dimensional PWR cores with both UO_2 and MOX fuels.

In both the 1-D and 2-D tests, fluxes in the coarse group solution improve considerably with only a few iterations and are shown to converge to the core fine group solutions after multiple iterations. Full convergence of the recondensation process was shown to be fully consistent with the multigroup methodology for a spatially flat flux approximation, but is by no means a substitute. The purpose of the recondensation technique is to substantially improve the coarse group solution with a minimal number of iterations.

Step difference spatial discretization is used in this study since it is consistent with the collapsing of the cross section moments which uses cell-averaged fluxes. A brief discussion is provided that explains the consistency of flat-flux approximation and the nature of the inconsistency for higher order spatial schemes.

References

1. D. R. ROBERTS, M. OUISLOUMEN, V. N. KUCUKBOYACI and K. N. IVANOV, " Development of Iterative Transport-Diffusion Methodology for LWR Analysis," *International conference on the Physics of Reactors, advances in Reactor Physics to Power the Nuclear Renaissance*, Pittsburgh, Pennsylvania, USA, May 9-14, 2010.

2. H. D. GOUGAR, "Results of a Neutronic Simulation of HTR-Proteus Core 4.2 Using PEBBED and Other INL Reactor Physics Tools: FY-09 Report," September 2009.

3. L. ZHU and B. FORGET, "A Discrete Generalized Multigroup Energy Expansion Theory," *Nuclear Science and Engineering*, **166**, 239 (2010).

4. B. FORGET and L. ZHU, "Mixed Energy Reactor Simulations using the Discrete Generalized Multigroup Method", *International conference on the Physics of Reactors, advances in Reactor Physics to Power the Nuclear Renaissance*, Pittsburgh, Pennsylvania, USA, May 9-14, 2010.

5. C. P. NEUMAN and D. I. SCHONBACH, "Discrete (Legendre) orthogonal polynomials—A Survey," *International Journal for Numerical Methods in Engineering*, **8**, 743 (1974).

6. E. E. LEWIS, G. PALMIOTTI, T. A. TAIWO, M. A. SMITH and N. TSOULFANIDIS, "Benchmark Specification for Deterministic 2-D/3-D MOX Fuel Assembly Transport Calculations without Spatial Homogenization (C5G7 MOX)," NEA/NSC/DOC(2010)4, March 28, 2001.

7. A. HEBERT, "Towards DRAGON Version4", *paper presented at the Topical Meeting on Advances in Nuclear Analysis and Simulation*, September 10-14, Vancouver, Canada (2006).

8. G. I. BELL and S. GLASSTONE, "Nuclear Reactor Theory," Van Nostrand Reinhold, New York (1970).

9. F. RAHNEMA, S. DOUGLASS, and B. FORGET, "Generalized Energy Condensation Theory," *Nucl. Sci. Eng.*, 160, **41** (2008).

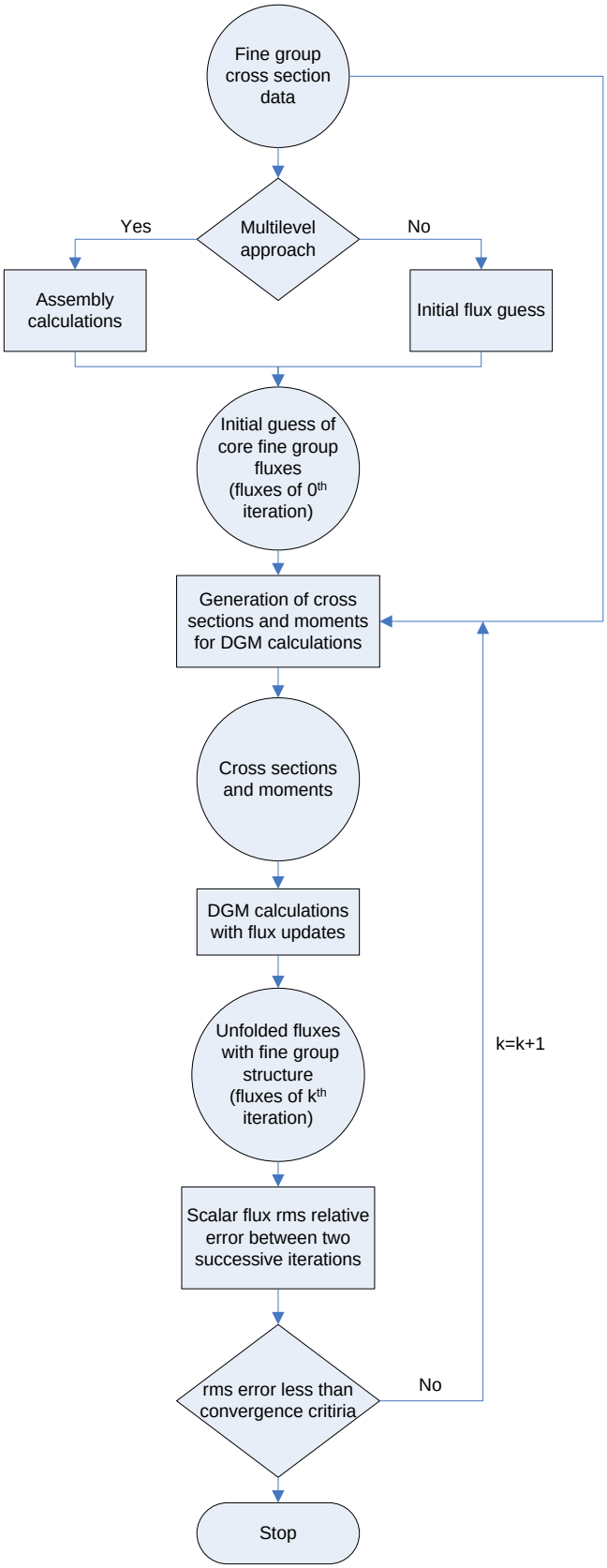

Fig. 1. Flow chart of the recondensation procedure.

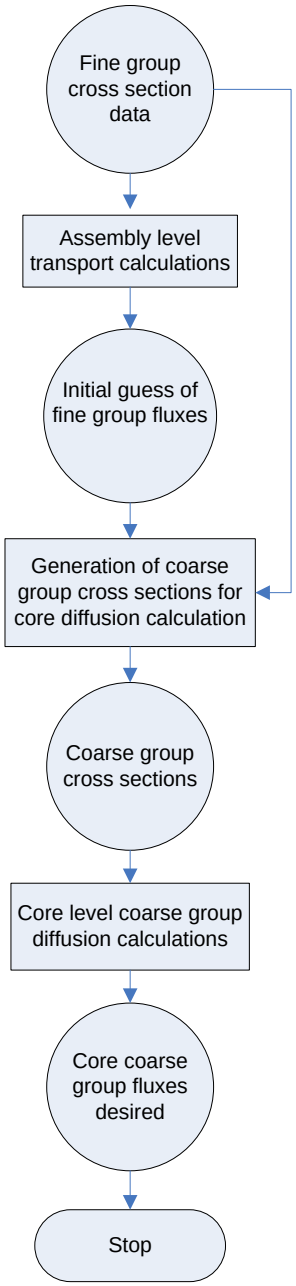

Fig. 2. Flow chart of the traditional multilevel procedure.

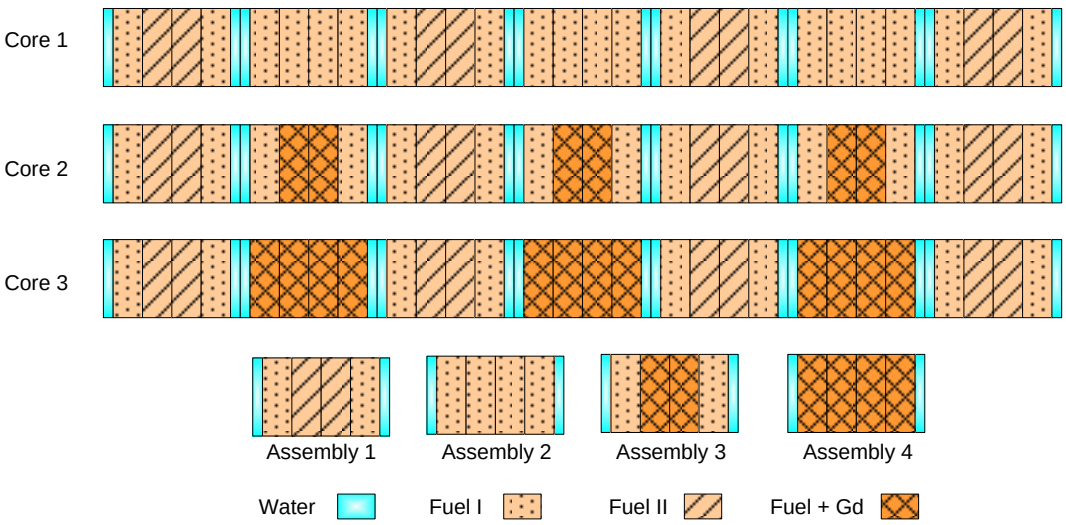

Figure 3. 1-D BWR core and assembly configurations.

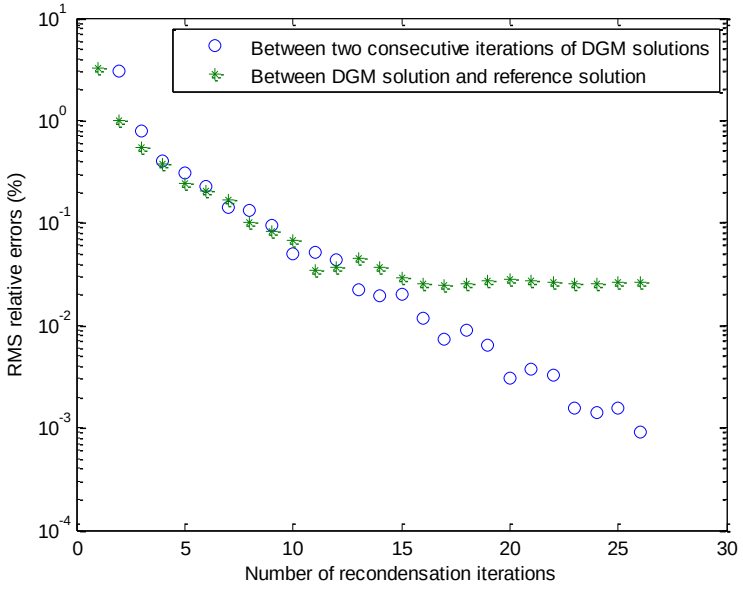

Fig. 4. Scalar flux *rms* relative errors of 1-D BWR core 1.

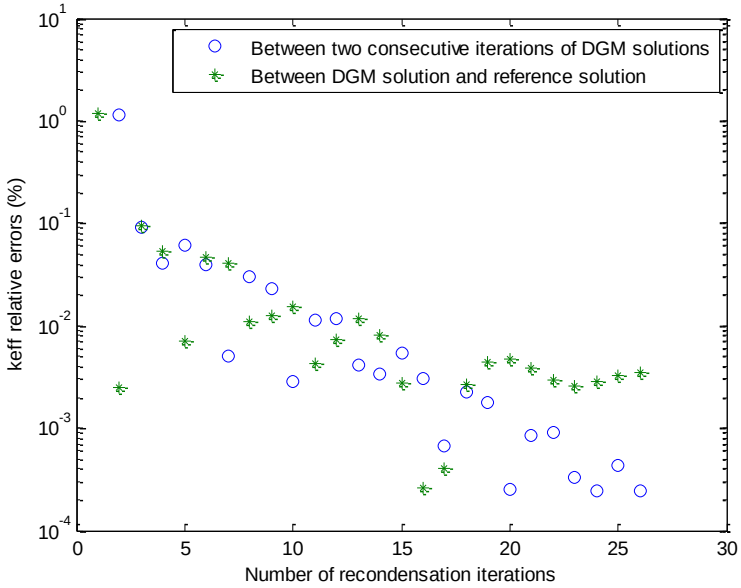

Fig. 5. Eigenvalue relative errors of 1-D BWR core 1.

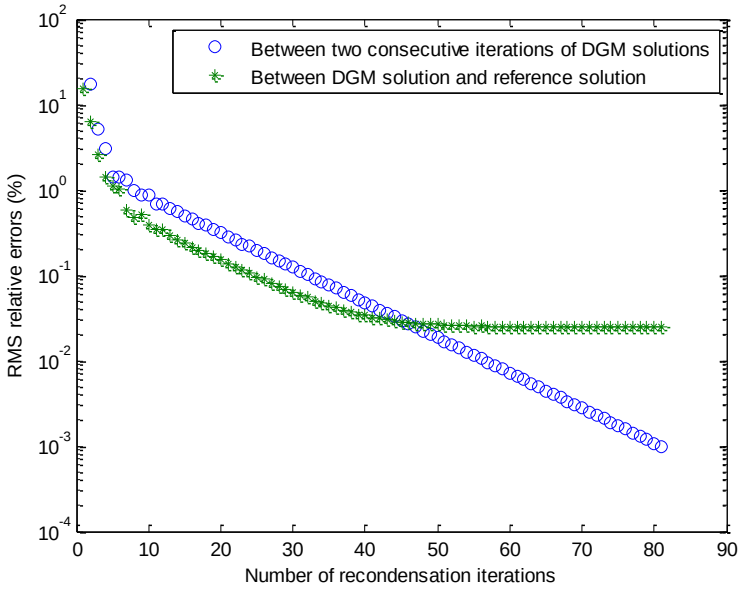

Fig. 6. Scalar flux *rms* relative errors of 1-D BWR core 3.

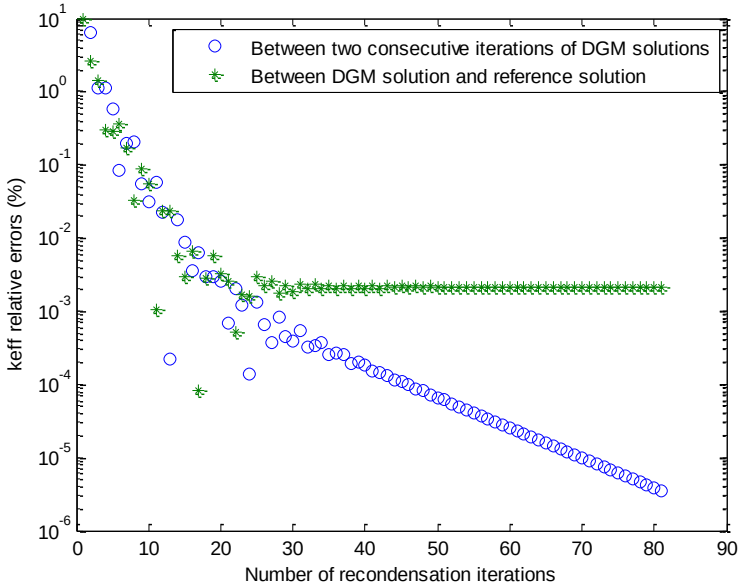

Fig. 7. Eigenvalue relative errors of 1-D BWR core 3.

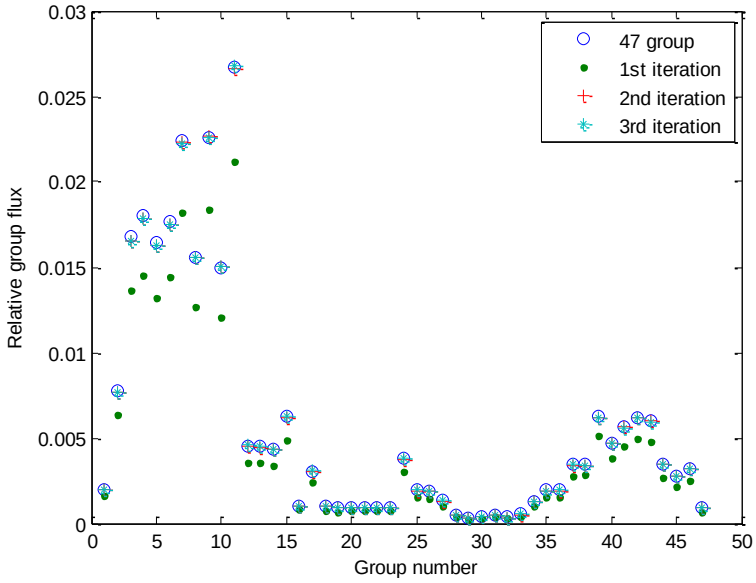

Fig. 8. Scalar flux comparison for core 3 water region.

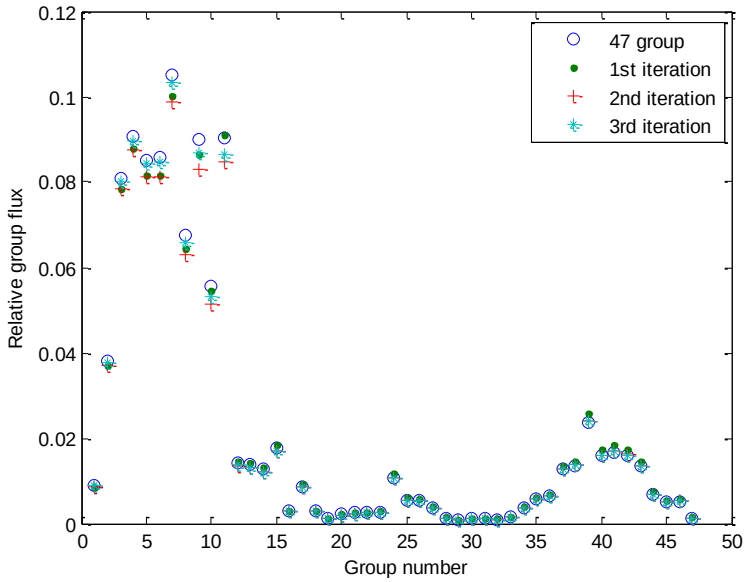

Fig. 9. Scalar flux comparison for core 3 Fuel (high enrichment) region.

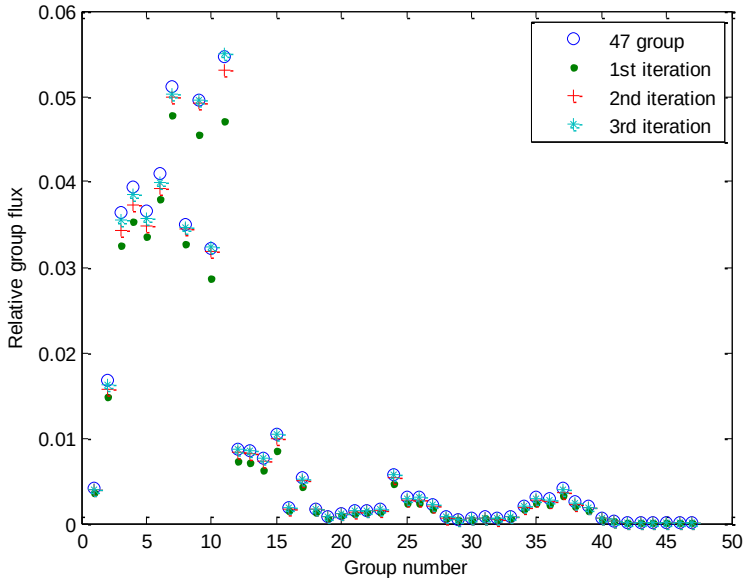

Fig. 10. Scalar flux comparison for core 3 Fuel+Gd region.

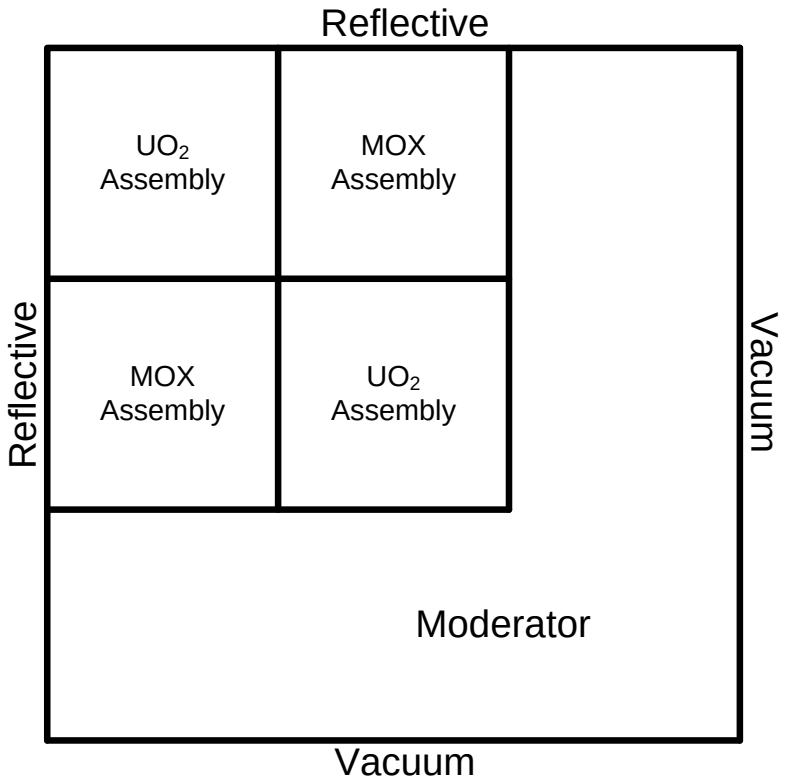

Fig. 11. 2-D PWR core configuration.

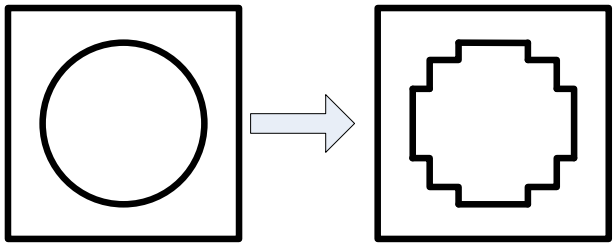
Fig. 12. Fuel pin approximation in Cartesian geometry.

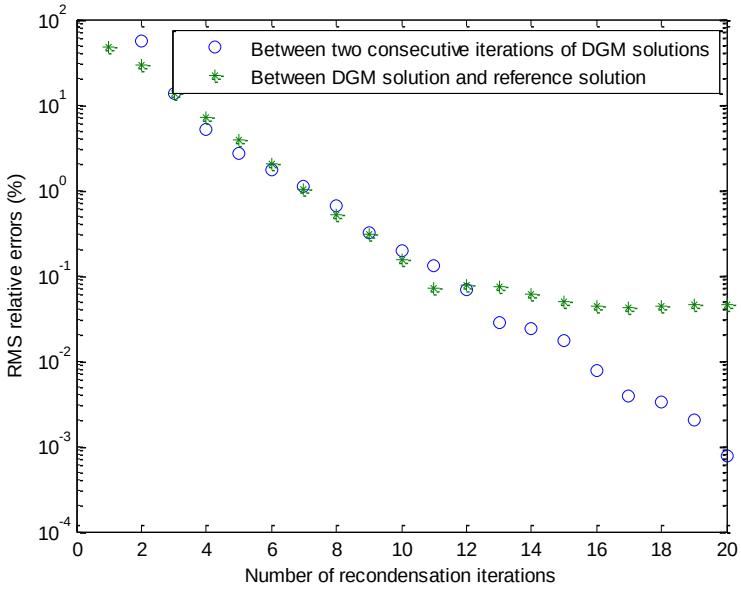

Fig. 13. Scalar flux *rms* relative errors of 2-D PWR core.

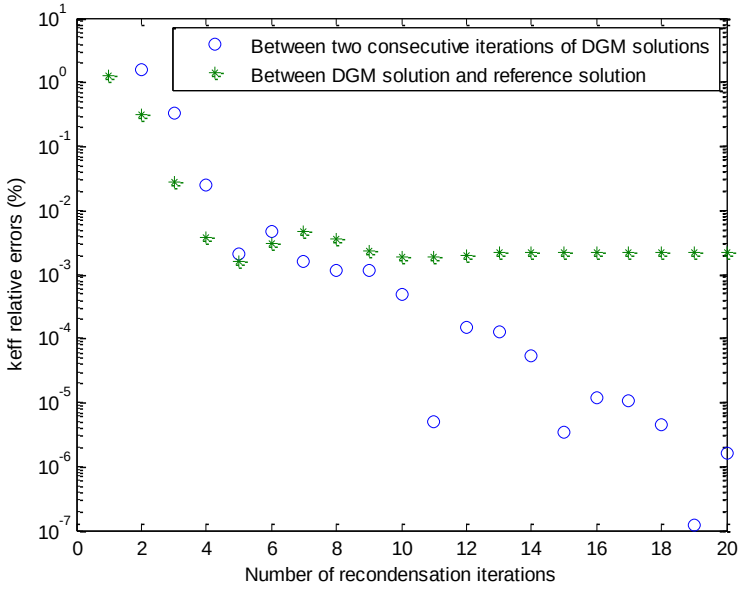

Fig. 14. Eigenvalue relative errors of 2-D PWR core.

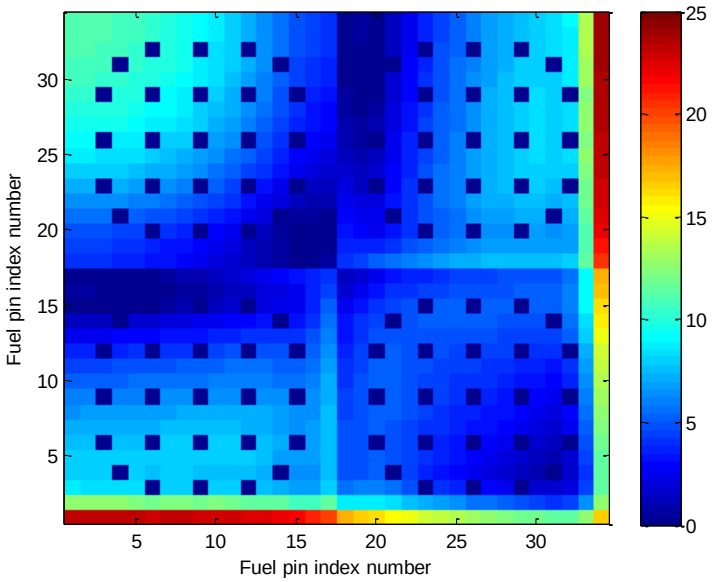

Fig. 15. Relative error (%) for 1st DGM iteration of pin power distribution of 2-D PWR core.

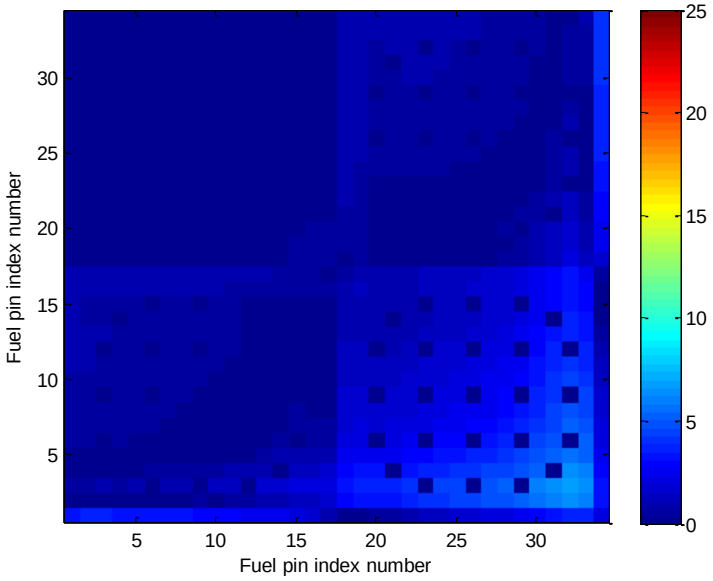

Fig. 16. Relative error (%) for 2nd DGM iteration of pin power distribution of 2-D PWR core.

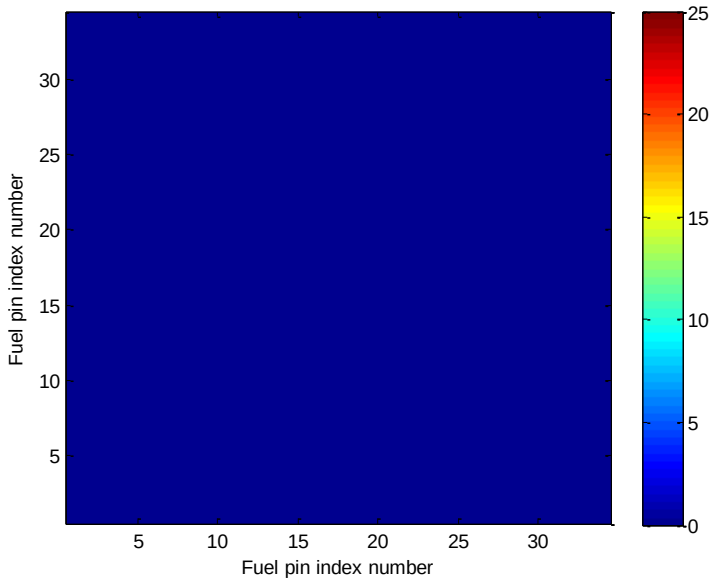

Fig. 17. Relative error (%) for 20th DGM iteration of pin power distribution of 2-D PWR core.

Table 1. 1-D BWR Core 1 computational results (errors in fluxes)

	rms (%)*	*mre* (%)*	*rms (%)*	*mre (%)*
1st iteration	-	-	3.2	1.6
2nd iteration	3.0	1.6	1.0	6.2E-1
3rd iteration	7.8E-1	3.9E-1	5.4E-1	2.9E-1
26th iteration	**8.9E-4**	4.5E-4	2.6E-2	1.6E-2

Note: Errors with * are between two consecutive iterations of DGM solution.
Errors without * are between DGM solution and reference solution.

Table 2. 1-D BWR Core 1 computational results (eigenvalue and computational time)

	Eigenvalue *k*	RE_k* (%)	RE_k (%)	Computation time *t (sec)*
1st iteration	1.16530	-	1.2	0.4
2nd iteration	1.15191	1.1	2.5E-3	0.8
3rd iteration	1.15296	9.2E-2	9.4E-2	1.2
26th iteration	1.15184	2.4E-4	3.5E-3	10.4
Reference solution	1.15188	-	-	10.4

Table 3. 1-D BWR Core 3 computational results (errors in fluxes)

	rms (%)*	*mre* (%)*	*rms (%)*	*mre (%)*
1st iteration	-	-	1.5E+1	8.5
2nd iteration	1.7E+1	6.4	6.4	4.3
3rd iteration	5.0	2.6	2.6	1.7
54th iteration	1.3E-2	**9.7E-4**	2.6E-2	1.6E-2
81st iteration	**9.7E-4**	7.5E-5	2.5E-2	1.2E-2

Table 4. 1-D BWR Core 3 computational results (eigenvalue and computational time)

	Eigenvalue *k*	RE_k* (%)	RE_k (%)	Computation time *t (sec)*
1st iteration	0.791960	-	9.6	0.4
2nd iteration	0.740744	6.5	2.6	0.8
3rd iteration	0.732551	1.1	1.4	1.2
54th iteration	0.722274	4.5E-5	2.1E-3	25.1
81st iteration	0.722274	3.4E-6	2.1E-3	37.4
Reference solution	0.722289	-	-	10.5

Table5. 2-D PWR Core computational results (errors in fluxes).

	rms (%)*	*rms (%)*	*mre (%)*
1st iteration	-	4.7E+1	7.6
2nd iteration	5.7E+1	2.9E+1	1.4
3rd iteration	1.4E+1	1.4E+1	6.3E-1
20th iteration	**7.6E-4**	4.6E-2	2.0E-2

Table 6. 2-D PWR Core computational results (errors in pin power).

	rms (%)	*mre (%)*	err_{max} *(%)*
1st iteration	7.3	6.0	24.1
2nd iteration	1.6	6.3E-1	6.9
3rd iteration	7.2E-1	3.0E-1	3.8
20th iteration	3.0E-2	2.0E-2	9.3E-2

Table 7. 2-D PWR Core computational results (eigenvalue and computational time).

	Eigenvalue *k*	RE_k* (%)*	RE_k *(%)*	Computational time *t (min)*
1st iteration	1.21074	-	1.3	7
2nd iteration	1.19213	1.5	3.1E-1	12
3rd iteration	1.19613	3.4E-1	2.8E-2	17
20th iteration	1.19577	1.6E-6	2.2E-3	101
Reference solution	1.19579	-	-	100